Divertor power spreading in the Divertor Tokamak Test facility for a full power scenario with Ar and Ne seeding

OPEN ACCESS
IOP Publishing
Plasma Physics and Controlled Fusion
Plasma Phys. Control. Fusion **65** (2023) 055009 (10pp)
https://doi.org/10.1088/1361-6587/acc2e3

Divertor power spreading in the Divertor Tokamak Test facility for a full power scenario with Ar and Ne seeding

I Ivanova-Stanik[1,*], P Chmielewski[1], Ch Day[2], P Innocente[3] and R Zagórski[4]

[1] Institute of Plasma Physics and Laser Microfusion, Hery 23, 01-497 Warsaw, Poland
[2] Karlsruhe Institute of Technology (KIT), Institute for Technical Physics, Karlsruhe, Germany
[3] Consorzio RFX (CNR, ENEA, INFN, Universit'a di Padova, Acciaierie Venete SpA), Padua, Italy
[4] National Centre for Nuclear Research (NCBJ), Otwock, Poland

E-mail: irena.ivanova-stanik@ifpilm.pl

Received 27 September 2022, revised 15 February 2023
Accepted for publication 9 March 2023
Published 31 March 2023

Abstract

This work describes integrated numerical modelling applied to Divertor Tokamak Test (DTT) scenarios with tungsten wall and divertor in single null configuration using the COREDIV code, which self-consistently solves 1D radial transport equations of plasma and impurities in the core region and 2D multi-fluid transport in the scrape-off layer (SOL). COREDIV code simulations have been performed and compared to the already published solutions from JETTO for DTT full power discharges with Ar seeding. The influence of the particle transport on the fuelling and flux to the plate is analysed. The main conclusion from the performed simulations is that Ne and Ar radiate effectively in the SOL and no difference was found in the fuelling properties between them. The fuelling increases with increase in radial transport in the core region. It has been found that the rise in the diffusion in the core plasma has a small influence on several global plasma parameters, such as plasma radiation, impurity concentration and fluxes to the divertor plate, but has a strong effect on the fuelling. The fuelling and deuterium flux to the plate decrease almost linearly with decreasing plasma density, keeping $\langle n_e \rangle / n_e^{sep} =$ constant.

Keywords: tokamak, DTT discharges, integrated modelling, impurity seeding

(Some figures may appear in colour only in the online journal)

1. Introduction

The development of a reliable solution for the power and particle exhaust in a fusion reactor is recognized as one of the main challenges towards the realization of a nuclear fusion power plant. In order to provide possible, reliable, well-assessed and on-time answers for DEMO, the Divertor Tokamak Test facility (DTT) [1] has been conceived and projected to be carried out and operated within the European strategy on fusion technology. For the DTT, one of the main missions is to study the power and particle exhaust issues in DEMO-relevant conditions. There are several methods to reduce power to the plate to lower than 10 MW m^{-2} such as by using liquid metal divertors, scrape-off layer (SOL) magnetic topology shaping to increase the wetted area, and impurity seeding.

The DTT should be able to operate with plasma bulk dimensionless parameters very close to those in DEMO and with a divertor region sufficiently flexible to test quite different magnetic divertor topologies, i.e. standard X point (single null (SN) configuration), double null configuration, snowflakes,

* Author to whom any correspondence should be addressed.

and different divertor materials (i.e. from tungsten to liquid metals) [2]. The divertor targets made of liquid metal, either lithium or tin, in highly powered tokamaks have been analysed in [3, 4].

Edge modelling of the DTT (tungsten divertor) low power, pure-D plasma scenario has been prepared and a quantitative comparison of the simulation results between three of the most popular edge codes, namely SOLPS-ITER, SOLEDGE2D and UEDGE, was reported in [5]. SOL and divertor modelling of the medium-density SN scenario of the DTT with tungsten divertor using the 2D coupled fluid-Monte Carlo code SOLEDGE2D-EIRENE for the deuterium case with impurity seeding have been presented in [6].

The DTT tokamak has been also analysed already by means of integrated COREDIV code simulations when either Li or Sn are applied as a liquid divertor target material [7] and with tungsten divertor [8].

For the optimization of various aspects of the DTT design, performing integrated modelling of foreseen operational scenarios is crucial and allows us to predict the non-linear feedback from plasma–wall interactions, heating, radiation, plasma fuelling and impurities (intrinsic and seeded) on discharge parameters.

This work describes integrated numerical modelling applied to the DTT scenarios with tungsten wall in SN divertor configuration using the COREDIV code [9], which self-consistently solves 1D radial transport equations for the main plasma and impurities in the core region and 2D multi-fluid transport in the SOL. We note that the COREDIV code has been successfully benchmarked against several JET discharges with a tungsten divertor and a beryllium wall (JET ILW) with nitrogen [10] and neon [11] seeding, and against ASDEX discharges (full tungsten machine) [12], proving its ability to reproduce the main features of seeded discharges.

The aim of this paper, which demonstrates the DTT simulations, is to support its design as well as to help in the development of a scientific work programme for a full power scenario (auxiliary heating about 45 MW, plasma current $I_\mathrm{p} = 5.5$ MA and toroidal magnetic field $B_\mathrm{T} = 6$ T). For these reasons, the work includes:

- analysis of the role of different transport coefficients on plasma parameters, reference core density and temperature profiles in the DTT obtained by 2D self-consistent modelling,
- determination of the necessary impurity seeding level for divertor protection for all cases,
- a matrix scan between different transport parameters and densities at the separatrix ($n_\mathrm{e}^\mathrm{sep}$) (density in range $4 \times 10^{19} \div 10 \times 10^{19}$ m^{-3}) as an indication of the range of possible operating conditions,.

The possible scenarios at full power of the proposed device have been analysed considering the aspect of safely handling the exhaust power on the divertor targets. Different to our previous work [8], here analysis is prepared for the cases with neon (Ne) and argon (Ar) seeding.

2. Physical model

Numerical simulations have been performed using the COREDIV code, which is based on an integrated approach coupling the radial transport in the core and the 2D multi-fluid description of the SOL. The interactions between seeded and intrinsic impurities significantly affect the particle and energy flows in the plasma. Therefore, a self-consistent approach is essential for a correct evaluation of the average power to the divertor plate.

In the core region, the energy and particle transport are defined by a local transport model, with a prescribed profile of transport coefficients, which considers barrier formation in the edge region in order to reproduce the energy confinement time calculated according to the currently valid scaling laws. More precisely, the ion and electron conductivities are defined by the formula: $\chi_\mathrm{e,i} = C_\mathrm{E}(a^2/\tau_\mathrm{E}) \times F(r)$, where a is the minor radius, τ_E is the energy confinement time obtained from the scaling law formula (IPB98$_{(y,2)}$) and the function $F(r)$ describes the parabolic-like profile of the conductivity coefficients with a drop near the separatrix due to H-mode barrier formation. The parameter C_E is adjusted to keep the calculated confinement time obtained from the simulations equal to the value defined by the scaling law in the absence of impurities. For all ions, background plasma and impurities, we have used the same anomalous transport coefficient defined by: $D_\mathrm{i} = \xi\, \chi_\mathrm{e,i}$ where D_i is an anomalous particle diffusion coefficient, $\chi_\mathrm{e,i}$ is an anomalous heat conductivity and the coefficient ς is an input parameter. For background plasma, we have used an anomalous pinch velocity defined by: $V_\mathrm{i}^\mathrm{pinch} = C_\mathrm{p}(D_\mathrm{i}\frac{r}{a^2})$ where C_p is the density peaking factor whose value for the main plasma ions has been chosen as a reference value in our simulations. It should be noted that the assumptions related to the profile of the transport coefficients are of secondary importance as long as the transport is such to keep the defined H_{98} factor, which is an input parameter in our simulations.

In the core, the source term takes into account the attenuation of the neutral density due to ionization processes: $S_\mathrm{i}(r) = S_\mathrm{i0}\exp(-\frac{a-r}{\lambda_\mathrm{ion}})$, where λ_ion is the penetration length of the neutrals, which is calculated self-consistently. The source intensity S_i0 is determined by the internal iteration procedure in such a way that the average electron density $\langle n_\mathrm{e}\rangle$ obtained from the neutrality condition is fixed (input parameter).

In the SOL, the 2D boundary layer code EPIT is used, which is primarily based on Braginskij-like equations for the DT plasma [13] and on rate equations for each ionization state of each impurity species. For every ion species, the continuity and the parallel momentum are considered and two energy equations (for T_e and common ion temperature T_i) are solved. Equations for different fluids are coupled by electrostatic, friction and thermal forces as well as by atomic processes such as collision ionization, recombination, excitation and charge exchange.

An analytical description of neutrals is employed based on a simple diffusive model, in order to avoid time-consuming Monte Carlo calculations. It takes into account the plasma (deuterium and seeded impurities) recycling in the divertor as

well as the sputtering processes at the target plates including deuterium sputtering, self-sputtering and sputtering due to seeded impurities. The recycling coefficient is an external parameter and the energy losses due to interactions with hydrogenic atoms (line radiation, ionization and charge exchange) are accounted for in the model. Note that the following definition of the recycling coefficient is used in our model: $R_{\mathrm{D}}^{\mathrm{cyc}} = 1 - \Gamma_{\mathrm{sep}}/\Gamma_{\mathrm{DIV}}$, where Γ_{DIV} is the total particle flux to the target and Γ_{sep} is the total flux crossing the separatrix. It should be underlined that the recycling coefficient in our approach includes effects related to the pumping efficiency (albedo) as well as the intensity of the puffing. In the case of seeded impurities (Ar, Ne) a constant value is assumed $R_{\mathrm{Ar,Ne}}^{\mathrm{cyc}} = 0.925$.

The Ar and Ne gas is puffed from the divertor region. We note that tungsten (W) is self-consistently calculated from sputtering at divertor targets due to all ions (main plasma and impurity). For deuterium and seeded impurity sputtering and tungsten self-sputtering, the yields given in [14] are used.

A simple slab geometry (poloidal and radial directions) with classical parallel transport and anomalous radial transport ($D_{\mathrm{i,perp}}^{\mathrm{SOL}} = \chi_{\mathrm{i}} = 0.5\chi_{\mathrm{e}}$) is used and the impurity fluxes and radiation losses caused by intrinsic and seeded impurity ions are considered in the model.

The coupling between the core and the SOL is made by imposing continuity of energy and particle fluxes as well as of particle densities and temperatures at the separatrix. The computed fluxes from the core are used as boundary conditions for the SOL plasma. In turn, the values of temperatures and of densities calculated in the SOL are used as boundary conditions for the core module.

3. Simulation results

Simulations are performed for the DTT full power scenario in SN configuration with the following main parameters: toroidal radius $R_{\mathrm{T}} = 2.19$ m and plasma radius $a = 0.7$ m. Different to our previous work [8] from 2017, here, plasma current (I_{p}) is lower ($I_{\mathrm{p}} = 5.5$ MA), toroidal magnetic field $B_{\mathrm{T}} = 6.0$ T, and elongation is -1.8 (similar to the parameters of the present European design of DEMO, aspect ratio $(R/a) = 3.1$). The average volume electron density is $\langle n_{\mathrm{e}}\rangle_{\mathrm{VOL}} = 0.91 \div 2.1 \times 10^{20}\,\mathrm{m}^{-3}$ and the separatrix density ($n_{\mathrm{e}}^{\mathrm{sep}}$) is kept at the 37% level of the volume average value ($n_{\mathrm{e}}^{\mathrm{sep}} = 0.37\langle n_{\mathrm{e}}\rangle_{\mathrm{VOL}}$), whereas the auxiliary total heating power is set to $P_{\mathrm{aux}} = 45$ MW.

The DTT is planned to be equipped with three auxiliary heating systems: a negative ion-based neutral beam injection system, an ion cyclotron resonance heating system with installed power up to 8 MW and an electron cyclotron resonance heating system with an installed power up to 32 MW [2]. In COREDIV code, we do not distinguish between different heating schemas and for the total auxiliary heating, a parabolic-like deposition profile is assumed. For this reason, we have compared the simulation with COREDIV code with the results of other code (JETTO), which has a more advanced model for auxiliary heating.

3.1. Comparison between the simulation results from COREDIV and JETTO codes

The first step is to analyse the case with $\langle n_{\mathrm{e}}\rangle_{\mathrm{VOL}} = 1.8 \times 10^{20}\,\mathrm{m}^{-3}$, for which JETTO simulations have been done and reported in [15, 16]. Note that in order to reproduce in our simulation the ratio between electron and ion temperatures in the centre $T_{\mathrm{e}}(0)/T_{\mathrm{i}}(0)$, $\chi_{\mathrm{i}} = 2.2\chi_{\mathrm{e}}$ has been used, while to reproduce the main plasma ion density the peaking factor $C_{\mathrm{p}} = 0.3$ has been applied in the case of background plasma. In the case of impurities, the peaking factor is twice as great. In our simulation, H_{98} is an input parameter for the COREDIV code and is equal to 0.85. The radial transport in the SOL has been assumed to be equal to $D_{\mathrm{i,perp}}^{\mathrm{SOL}} = 0.5\,\mathrm{m}^2\,\mathrm{s}^{-1}$ in order to reproduce the total radiation and the core radiation. The choice of $D_{\mathrm{i,perp}}^{\mathrm{SOL}} = 0.5\,\mathrm{m}^2\,\mathrm{s}^{-1}$ is consistent with our previous simulations for the JET ILW [17, 18].

The comparison between COREDIV and JETTO results for the case with Ar seeding for the same effective charge state (Z_{EFF}) of about 1.8 is presented in figure 1. Relatively good agreement between JETTO and COREDIV simulations can be seen for densities (figure 1(a)), temperatures (figure 1(d)) and Z_{EFF} (figure 1(c)) profiles. In figure 1(f) radiation from the JETTO simulation is presented which takes into account only W radiation in the core plasma.

The Ar concentration (C_{Ar}) in both numerical cases is similar: 0.247% from COREDIV and 0.28% from JETTO. Regarding W density (see figure 1(e)), strong picking at the separatrix for the JETTO simulation is observed, whereas similar values are seen in the bulk region (figure 1(e)). There is, however, a large difference in the radiation profiles of W (see figure 1(f)). This difference might be caused by different W atomic data used in the codes (COREDIV uses the W data obtained from T. Putterich). According to the COREDIV simulations, the Ar radiation has two peaks: one at the separatrix and the second one at $r/a = 0.8$. The maximum of the W radiation is at $r/a = 0.85$, which is outside the pedestal region. In the JETTO simulation [15], the total neutron rate amounts to 1.47×10^{17} neutrons s^{-1}, which is in good agreement with the COREDIV data (1.57×10^{17} neutrons s^{-1}). We note that the power to the plate (P^{PLATE}), calculated by COREDIV (see figure 2(b)) and corresponding to the JETTO case, is 10 MW, which is an acceptable value for the DTT.

3.2. Analysis of the influence of different transport on plasma performance

The influence of the radial transport in the SOL has been analysed in many papers for different devices with different codes, for ITER (with SOLPS [19] and COREDIV [20]) and ASDEX Upgrade (with SOLPS [21] and COREDIV [22]). In order to investigate the influence of radial transport in the SOL on the DTT workspace, simulations with Ar and Ne seeding for the same discharge parameters have been performed. We have performed simulations for two different values of radial diffusion in the SOL $D_{\mathrm{i,perp}}^{\mathrm{SOL}} = 0.5\,\mathrm{m}^2\,\mathrm{s}^{-1}$ and $0.25\,\mathrm{m}^2\,\mathrm{s}^{-1}$. The value of $D_{\mathrm{i,perp}}^{\mathrm{SOL}}$ is constant in space. We note that $D_{\mathrm{i,perp}}^{\mathrm{SOL}} = 0.5\,\mathrm{m}^2\,\mathrm{s}^{-1}$ is used in [8], but for the case with nitrogen and Ar seeding.

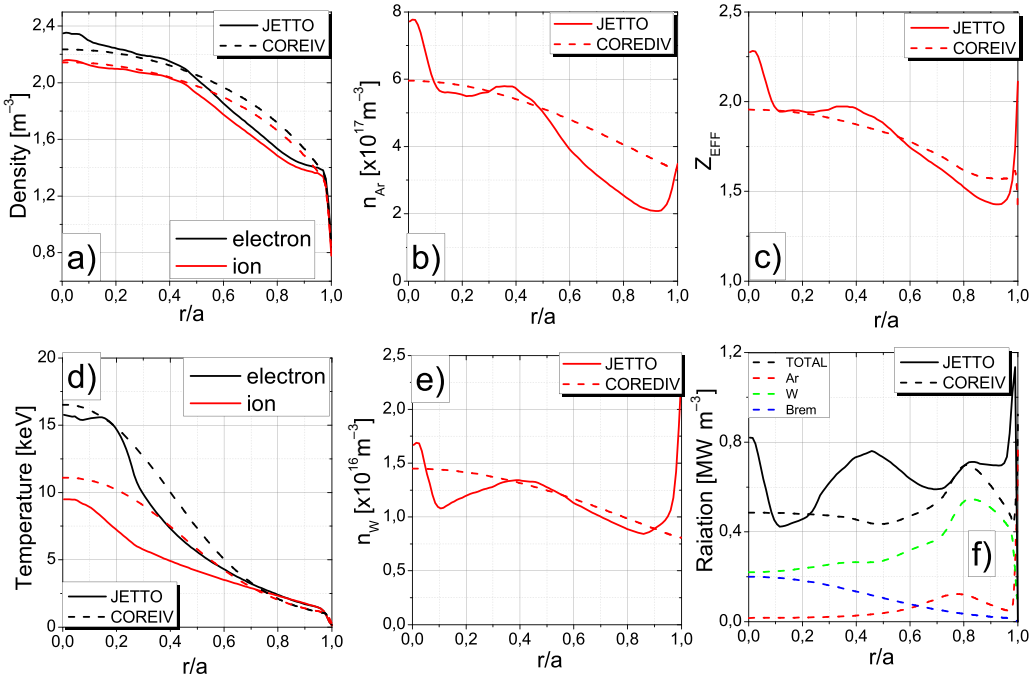

Figure 1. The electron (a), Ar (b), W (e) densities, electron and ion temperatures (d), Z_{EFF} (c) and total and impurities radiation profiles in the core (f) for the case with Ar seeding $\langle Z_{EFF} \rangle = 1.8$.

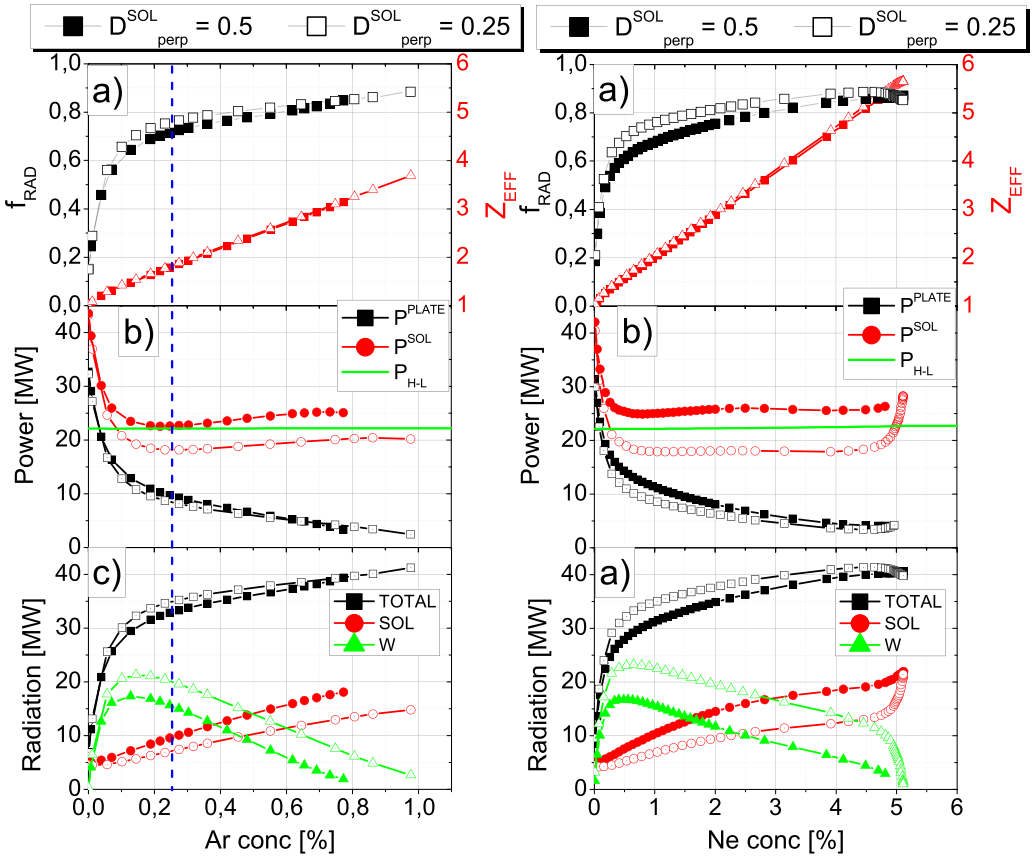

Figure 2. Plasma parameters versus Ar (left) and Ne (right) concentration for two different values of radial diffusion in SOL $D^{SOL}_{perp} = 0.5\,m^2\,s^{-1}$ (full symbol) and $0.25\,m^2\,s^{-1}$ (open symbol): (a) radiation fraction and Z_{EFF}, (b) power to plate (P^{PLATE}), to SOL (P^{SOL}) and H–L power threshold (P_{HL}) and (c) radiation in the SOL, W radiation in the core and total radiation. The vertical blue line marks the case which is compared to JETTO simulations.

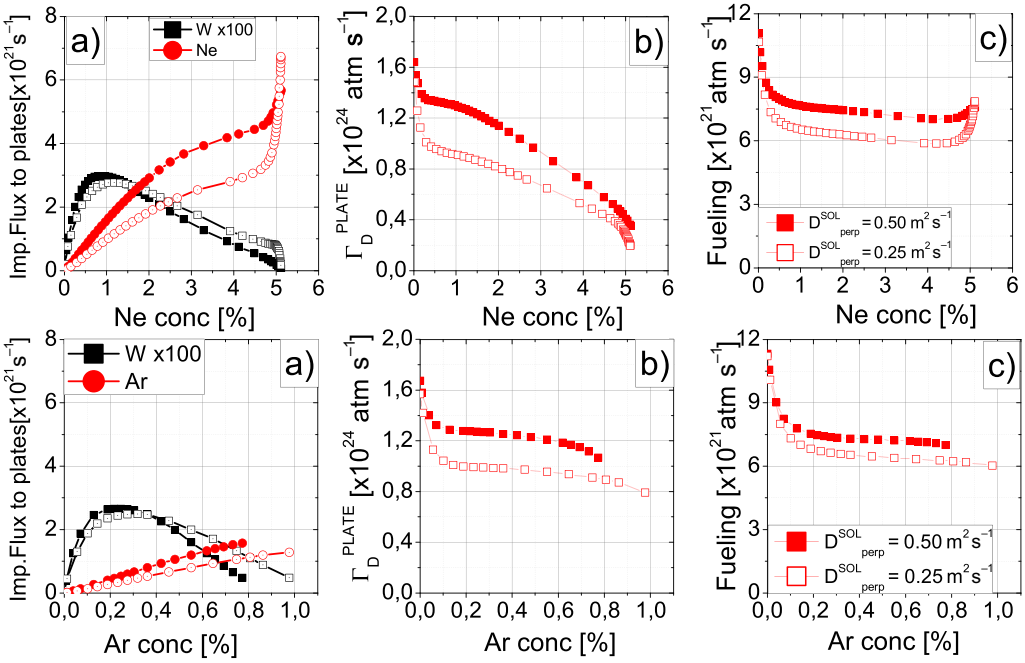

Figure 3. Impurities and deuterium flux to the plate ($\Gamma_{\mathrm{D}}^{\mathrm{PLATE}}$) and fuelling vs impurity concentration Ne (top panel) and Ar (bottom panel) for the case $n_{\mathrm{es}}^{\mathrm{mid}} = 8.71 \times 10^{19}\,\mathrm{m}^{-3}$ with two different values of radial diffusion in the SOL.

Figure 2 shows the main plasma parameters vs Ar (left) and Ne (right) concentrations for the case with density at the separatrix at the midplane position, $n_{\mathrm{es}}^{\mathrm{mid}} = 8.71 \times 10^{19}\,\mathrm{m}^{-3}$ (JETTO case). It can be seen that for the case with higher radial transport in the SOL the screening efficiency of the edge region is improved leading to lower W radiation (see figure 2(c)) in the core plasma. Consequently, higher P^{PLATE} is observed and the power crossing the separatrix (P^{SOL}) is higher than the L–H transition power threshold (P_{HL}) calculated by Martin law [23]. We note that based on [23] the power threshold depends on the line-average electron density, toroidal magnetic field and surface. For DTT, we have two times higher density in comparison to JET ILW and ASDEX Upgrade and about two times higher toroidal magnetic field. Therefore, the L–H power threshold for DTT is much higher than for JET ILW and ASDEX and is equal to about 22 MW.

For the case with lower diffusion ($D_{\mathrm{i,perp}}^{\mathrm{SOL}} = 0.25\,\mathrm{m}^2\,\mathrm{s}^{-1}$), there is no possibility to work in H-mode with Ar seeding with acceptable power to the plate (<10.0 MW), because $P^{\mathrm{SOL}} < P_{\mathrm{HL}}$ (see figure 2(b)). However, for the case with Ne seeding with $D_{\mathrm{i,perp}}^{\mathrm{SOL}} = 0.25\,\mathrm{m}^2\,\mathrm{s}^{-1}$ it might be possible to work in H-mode with acceptable power to the plate only for very strong seeding, where Ne concentration (C_{Ne}) is >5% see (figure 2(a)) with, however, very large Z_{EFF} values (of about 5.5). The reason for this difference in power to the SOL for the highest Ne and Ar seeding levels is related to a large part of Ar radiation being in the core. For the case with $C_{\mathrm{Ar}} = 0.97\%$, Ar radiation in the core is 17.7 MW, which is more than twice that of the case with the maximum Ne puff level.

We note that for the case without impurity seeding the radiation fraction is only equal to 0.16 and P^{PLATE} is 36.5 MW, which is not a technologically allowed value. Therefore, impurity seeding is obligatory to reduce power to the plate to an acceptable level. The temperature at the strike point at the divertor plate ($T_{\mathrm{e}}^{\mathrm{PLATE}}$) is 9.7 eV. Note that low-temperature conditions in the divertor do not guarantee a strong enough reduction in the power to the target plates and the divertor heat load might be tolerable only for the higher seeding levels, again mostly due to reduction of the input power with increased seeding.

The simulations with COREDIV code are run to the steady-state phase of the discharges with constant-volume electron density (input parameter). In order to keep $\langle n_{\mathrm{e}} \rangle_{\mathrm{VOL}}$ constant, the level of the fuelling intensity is determined by an internal iteration procedure in such a way that the average electron density obtained from the neutrality condition is equal to a prescribed value. The impurity seeding has an influence on the fuelling source, because impurities are ionized in the plasma and, in order to fulfil the quasi-neutrality condition, the main ion density is decreased. Consequently, the total rate at which the main ions leave the plasma decreases and consequently the requested fuelling rate.

In figure 3, impurities and deuterium fluxes to the plate ($\Gamma_{\mathrm{D}}^{\mathrm{PLATE}}$) and fuelling (deuterium source) vs impurity concentration, Ne (top panel) and Ar (bottom panel), for the cases with two different radial diffusion values in the SOL are presented. Doubling of the radial diffusion in SOL leads to a change in deuterium flux to the plate, which decreases by about 20%. It is found that the deuterium flux to the plate is reduced by a factor of 2 in the case of Ar seeding and 3 in the case of Ne seeding, when moving from the case without impurity seeding to the case with maximum impurity seeding level. With the increase in the impurity seeding, the fuelling source decreases and for the highest seeding level goes to the

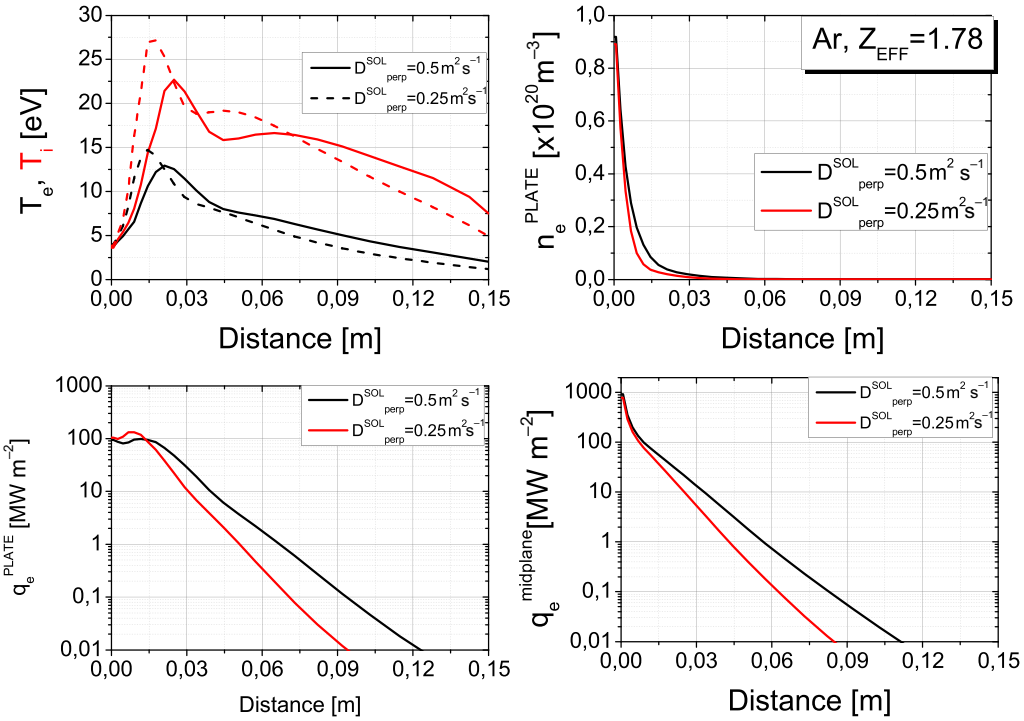

Figure 4. Simulated profiles of the electron density, electron and ion temperatures, q_e^{PLATE} and $q_e^{midplane}$ at the target plate (right) for the case with Ar seeding, $\langle Z_{EFF}\rangle = 1.78$.

same level for both impurities at about $6-7\times10^{21}$ atm s^{-1}. It appears that the transport in the SOL has a small influence on the fuelling for $C_{Ar} > 0.2\%$ (see figure 3(c)). It should be noted that for $C_{Ar} > 0.2\%$ tungsten is replaced by Ar.

In figure 4, simulated radial profiles are presented of the electron density, the electron and ion temperatures at the target plate, and the heat flux to the plate (q_e^{PLATE}) and at the midplane ($q_e^{midplane}$) for the case with Ar seeding, $\langle Z_{EFF}\rangle = 1.78$. The plasma is in a semi-detached phase: the maximum of the temperature is shifted to the wall. The semi-detachment is defined in our simulations as a significant reduction of the heat flux and pressure along field lines between the midplane and divertor target, but only in the part of the target plate close to the strike point (see [24] for details). We observe, that with decrease of the radial transport, the profiles of the electron density, q_e^{PLATE} and $q_e^{midplane}$ at the plate are narrower, indicating smaller e-folding lengths. However, since the SOL is modelled by a simple slab geometry (poloidal and radial directions) which neglects both the real divertor geometry and a possible flux expansion at the plate, only the total divertor load is considered in the following and not its distribution along the target.

In the next step, the influence of the transport in the core on the DTT working parameters in the cases of Ar and Ne seeding for fixed separatrix plasma density is investigated. The ratio between particle diffusion and the heat conductivity coefficient in the core plasma is a free parameter for the transport simulations in our model. To assess how the assumption about particle transport in the core influences the simulation results, two different values of the ratio of particle diffusion coefficient to thermal electron conductivity, $\xi = 0.1$ and 0.35, have been used.

In figure 5, impurity and deuterium fluxes to the plate, tungsten concentration in the core (C_W), electron density and temperature at the strike point at the plate, SOL and W radiation, bremsstrahlung and fuelling versus Ar concentration are presented.

Simulations show that with the decrease of the particle diffusion coefficient relative to the thermal electron conductivity in the core one can observe a strong change in the fuelling (a decrease by about a factor of 3), but a relatively small influence on the particle fluxes to the plate, Z_{EFF} and radiation. We note that the fuelling value 2.5×10^{21} atm s^{-1} for the case of $\xi = 0.1$ is similar to the value 3.6×10^{21} atm s^{-1} which is reported in [15]. However, it should be pointed out that particle diffusion coefficient in core might affect strongly the fusion reactor performance, where the effect of helium ash accumulation could be important as reported in [25].

3.3. Analysis of the influence of different plasma densities on plasma performance

As an indication of the range of possible operating conditions, a matrix scan for different transport parameters and densities at the separatrix has been performed for separatrix density in the range $4\times10^{19} \div 10\times10^{19}$ m^{-3} keeping the ratio $\langle n_e\rangle_{VOL}/n_e^{sep}$ constant. In figure 6, the main plasma parameters for five different densities are presented. It can be seen that for the case with Ar seeding the W radiation is replaced by Ar radiation and, as a consequence, the W radiation in the core for the

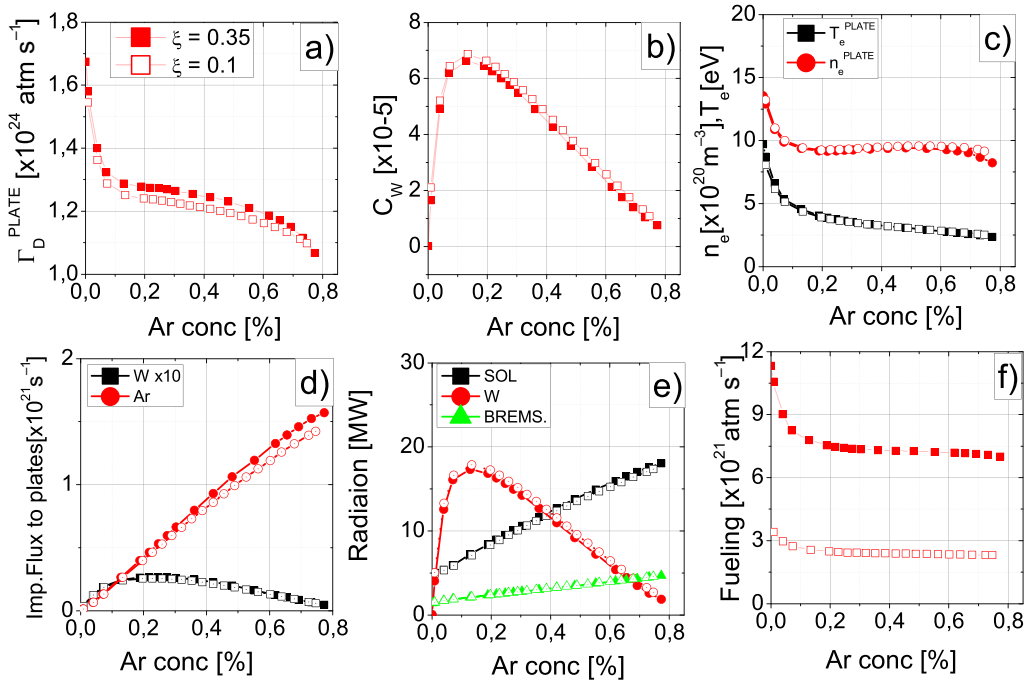

Figure 5. Plasma parameters versus Ar concentration: (a) deuterium flux to the plate, (b) tungsten concentration in core (C_W), (c) electron density and temperature at the strike point at the plate, (d) impurities flux to the plate, (e) SOL and W radiation, bremsstrahlung and (f) fuelling.

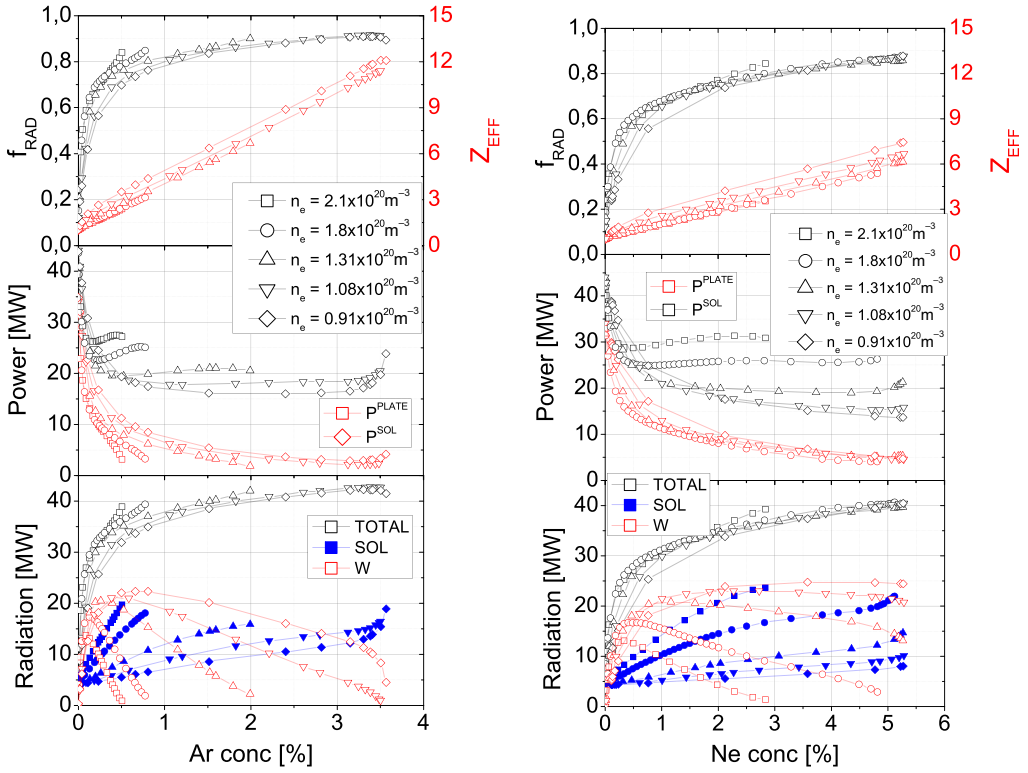

Figure 6. Plasma parameters versus Ar (left) and Ne (right) concentration with a radial diffusion coefficient in the SOL of $D_{\mathrm{perp}}^{\mathrm{SOL}} = 0.5\,\mathrm{m}^2\,\mathrm{s}^{-1}$: radiation fractio($\mathrm{f_{RAD}}$) and Z_{EFF}, power to plate($\mathrm{P^{PLATE}}$), to SOL)$\mathrm{P^{SOL}}$)and radiation in SOL, W radiation in the core, and total radiation for the case with different plasma density.

Table 1. Main parameters of the DTT full power scenario with Ar seeding with different separatrix density for two values of radial diffusion in the SOL, $D_{\rm perp}^{\rm SOL} = 0.5\,{\rm m^2\,s^{-1}}$ and $D_{\rm perp}^{\rm SOL} = 0.25\,{\rm m^2\,s^{-1}}$ (in parentheses).

Parameter	$n_{\rm es}^{\rm mid}$ $10\times10^{19}\,{\rm m^{-3}}$	$n_{\rm es}^{\rm mid}$ $8.7\times10^{19}\,{\rm m^{-3}}$	$n_{\rm es}^{\rm mid}$ $6.5\times10^{19}\,{\rm m^{-3}}$	$n_{\rm es}^{\rm mid}$ $5.4\times10^{19}\,{\rm m^{-3}}$	$n_{\rm es}^{\rm mid}$ $4.6\times10^{19}\,{\rm m^{-3}}$
$\langle n_{\rm e}\rangle$ ($\times10^{20}$ m^{-3})	2.1	1.8	1.31	1.08	0.91
$R^{\rm TOTAL}$ (MW)	32.9 (33.2)	32.8 (33.67)	33.8 (33.1)	34.1 (34.1)	33.7 (32.9)
$R_{\rm Ar}^{\rm CORE}$ (MW)	7.13 (4.19)	4.7 (3.50)	3.6 (2.0)	3.4 (2.25)	2.64 (1.52)
$R_{\rm W}^{\rm CORE}$ (MW)	8.62 (19.4)	15.9 (21.1)	20.0 (24.6)	21.0 (25.2)	22.3 (24.5)
$C_{\rm W}$ ($\times10^{-5}$)	2.32 (5.10)	6.0 (8.0)	16.4 (19.5)	28.2 (32.5)	46.6 (49.6)
$C_{\rm Ar}$ (%)	0.27 (0.16)	0.3 (0.19)	0.39 (0.22)	0.58 (0.39)	0.62 (0.38)
$Z_{\rm EFF}$	1.77 (1.52)	1.78 (1.66)	2.42 (2.0)	3.26 (2.77)	3.97 (3.22)
$P^{\rm SOL}$ (MW)	26.6 (19.2)	22.6 (18.4)	19.5 (16.83)	18.6 (15.8)	18.2 (17.4)
$P_{\rm LH}$ (MW)	24.6	22.1	17.9	15.68	13.9
$P^{\rm PLATE}$ (MW)	10.1 (10.8)	10.7 (10.5)	10.0 (11.0)	10.0 (10.3)	10.6 (11.4)
$T_{\rm e}^{\rm PLATE}$ (eV)	3.07 (3.8)	3.75 (4.23)	4.5 (6.0)	4.6 (6.1)	5.6 (7.98)

Table 2. Main parameters of the DTT full power scenario with Ne seeding with different separatrix density for two values of radial diffusion in the SOL, $D_{\rm perp}^{\rm SOL} = 0.5\,{\rm m^2\,s^{-1}}$ and $D_{\rm perp}^{\rm SOL} = 0.25\,{\rm m^2\,s^{-1}}$ (in parentheses).

Parameter	$n_{\rm es}^{\rm mid}$ $10\times10^{19}\,{\rm m^{-3}}$	$n_{\rm es}^{\rm mid}$ $8.7\times10^{19}\,{\rm m^{-3}}$	$n_{\rm es}^{\rm mid}$ $6.5\times10^{19}\,{\rm m^{-3}}$	$n_{\rm es}^{\rm mid}$ $5.4\times10^{19}\,{\rm m^{-3}}$	$n_{\rm es}^{\rm mid}$ $4.6\times10^{19}\,{\rm m^{-3}}$
$\langle n_{\rm e}\rangle$ ($\times10^{20}$ m^{-3})	2.1	1.8	1.31	1.08	0.91
$R^{\rm TOTAL}$ (MW)	32.9 (32.9)	33.2 (33.7)	33.3 (34.0)	33.7 (33.8)	33.76 (34.4)
$R_{\rm Ne}^{\rm CORE}$ (MW)	3.7 (2.0)	3.0 (1.63)	1.94 (1.17)	1.67 (1.0)	1.46 (1.0)
$R_{\rm W}^{\rm CORE}$ (MW)	7.35 (19.6)	13.6 (23.1)	20.6 (25.8)	22.8 (26.4)	23.7 (26.8)
$C_{\rm W}$ ($\times10^{-5}$)	2.08 (5.27)	5.5 (8.8)	17.6 (20.9)	31.8 (34.7)	53.6 (56.6)
$C_{\rm Ne}$ (%)	1.14 (0.75)	1.5 (0.78)	1.6 (0.96)	1.85 (1.13)	2.12 (1.64)
$Z_{\rm EFF}$	2.28 (1.76)	2.44 (1.86)	2.8 (2.28)	3.38 (2.77)	4.21 (3.8)
$P^{\rm SOL}$ (MW)	30.4 (20.6)	25.4 (18.4)	20.3 (16.23)	18.4 (15.8)	17.6 (15.2)
$P_{\rm LH}$ (MW)	24.6	22.1	17.9	15.68	13.9
$P^{\rm PLATE}$ (MW)	10.4 (11.2)	10.4 (10.4)	10.8 (10.4)	10.6 (10.8)	10.8 (10.3)
$T_{\rm e}^{\rm PLATE}$ (eV)	3.28 (4.0)	4.08 (4.7)	5.24 (6.0)	5.41 (6.6)	6.46 (7.4)

highest seeding level decreases to $1 \div 2$ MW. We observe that, after a strong initial increase of the W radiation (density) with increase of the impurity puff level, there is a slow decrease in the W radiation. In the case with Ne seeding, a strong reduction of about 50% of the W radiation is observed only for the highest levels of $n_{\rm e}$ ($1.8\times10^{20}\,{\rm m^{-3}}$ and $2.1\times10^{20}\,{\rm m^{-3}}$). This reduction is the effect of the higher plasma density and lower temperature in the divertor, which leads to higher radiation in the SOL for this same level of the Ne gas puff.

In table 1, the main plasma parameters as total radiation ($\rm R^{TOTAL}$), W ($\rm R^{CORE}{}_W$) and Ar ($\rm R^{CORE}{}_{Ar}$) radiation in core pasma are given for the case with Ar seeding for both radial diffusion coefficients in the SOL, $0.5\,{\rm m^2\,s^{-1}}$ and $0.25\,{\rm m^2\,s^{-1}}$ (in parentheses), and for similar power to the divertor plate in the range of 10–11 MW.

From table 1, with the decrease of the separatrix density, the Ar concentration increases about 2.5 times, but argon radiation in the core ($R_{\rm Ar}^{\rm CORE}$) decreases from 7.13 MW to 2.64 MW. The temperature of the plate ($T_{\rm e}^{\rm PLATE}$) increases going to higher W production leading to higher $C_{\rm W}$ and radiation from W in the core changing from 8.62 MW to 22.3 MW. We point out the increase in tungsten radiation (by a factor of 2) when the density is reduced from $10\times10^{19}\,{\rm m^{-3}}$ to only $8.7\times10^{19}\,{\rm m^{-3}}$. There is no problem to work in H-mode for the case with $D_{\rm perp}^{\rm SOL} = 0.5\,{\rm m^2\,s^{-1}}$. For lower diffusion, working with $P^{\rm SOL} > P_{\rm LH}$ is possible only for low plasma densities, $n_{\rm es}^{\rm mid} \leqslant 5.4\times10^{19}\,{\rm m^{-3}}$.

In table 2, the main plasma parameters are presented for the case with Ne seeding for both radial diffusion coefficients in the SOL, $0.5\,{\rm m^2\,s^{-1}}$ and $0.25\,{\rm m^2\,s^{-1}}$ (in parentheses) and for a similar power to the divertor plate, ∼10–11 MW .

Comparing Ar and Ne seeding cases, the behaviour of the W concentration and radiation in the core changes very little in both cases: it increases with the decrease in the density. For the case with Ne seeding, for the same density, we observe lower $C_{\rm W}$ by about 10%, which is the consequence of lower sputtering. Ne radiation in the core ($R_{\rm Ne}^{\rm CORE}$) is about $1.5 \div 2$ times lower in comparison with Ar seeding.

In figure 7, the fuelling and the deuterium flux to the plate are shown for a similar power to the divertor plate, about 10–11 MW, for Ne and Ar seeding.

The fuelling changes strongly with the separatrix density from 3×10^{21} 1/s to $7.5 \div 9\times10^{21}$ 1/s, depending on the diffusion coefficient. We note that radial diffusion in the SOL has almost no influence on the fuelling for low plasma densities ($<8\times10^{19}\,{\rm m^{-3}}$) and for the highest density the difference

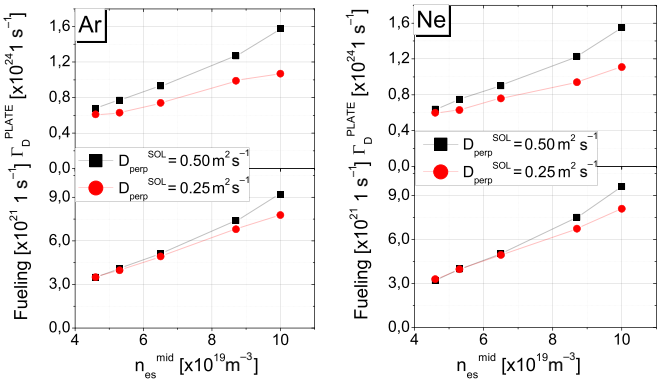

Figure 7. Fuelling and deuterium flux to the plate versus separatrix density for the case with Ar (left) and Ne (right).

reaches about 15%. The influence of radial diffusion in the SOL is stronger on the $\Gamma_{\mathrm{D}}^{\mathrm{PLATE}}$ and the difference reaches about 25%–30% for the highest densities. The fuelling and $\Gamma_{\mathrm{D}}^{\mathrm{PLATE}}$ decrease almost linearly with decreasing plasma density, keeping $\langle n_{\mathrm{e}}\rangle/n_{\mathrm{es}}^{\mathrm{mid}} = \text{constant}$.

4. Conclusions

COREDIV code has been used to simulate DTT full power discharges with different transport in the core and the SOL region with Ar and Ne impurity seeding, with a particular focus on the influence of impurity seeding and transport on the fuelling and particle fluxes to the plate. We have good agreement between JETTO and COREDIV simulations for densities, temperatures and Z_{EFF} profiles. Results show that low-temperature conditions in the divertor do not guarantee a strong enough reduction in the power to the target plates and the divertor heat load might be tolerable only for the middle seeding levels, mostly due to reduction of the input power with increased seeding.

From the results of the simulations with constant electron density at the separatrix, it is found that the fuelling source is reduced by a factor of 2 in the case with Ar seeding and 3 in the case with Ne seeding, when moving from lowest to highest seeding level. The fuelling particle source, $\Gamma_{\mathrm{D}}^{\mathrm{PLATE}}$ decreases linearly with the decrease in the density, when $\langle n_{\mathrm{e}}\rangle/n_{\mathrm{e}}^{\mathrm{sep}} = \text{constant}$.

For Ar and Ne seeding, it is possible to achieve H-mode plasma operation ($P^{\mathrm{SOL}} > P_{\mathrm{L-H}}$) with an acceptable level of power to the target plates for the case with highest radial diffusion in the SOL ($D_{\mathrm{perp}}^{\mathrm{SOL}} = 0.5\,\mathrm{m^2\,s^{-1}}$).

Data availability statement

All data that support the findings of this study are included within the article (and any supplementary files).

Acknowledgments

This work has been carried out within the framework of the EUROfusion Consortium, funded by the European Union via the Euratom Research and Training Programme (Grant Agreement No. 101052200—EUROfusion). Views and opinions expressed are however those of the author(s) only and do not necessarily reflect those of the European Union or the European Commission. Neither the European Union nor the European Commission can be held responsible for them.

This scientific paper has been published as part of the international project co-financed by the Polish Ministry of Science and Education within the programme called 'PMW' for 2022–2023.

ORCID iDs

I Ivanova-Stanik https://orcid.org/0000-0002-2766-8612
P Chmielewski https://orcid.org/0000-0002-1412-6769
R Zagórski https://orcid.org/0000-0003-3491-2545

References

[1] Martone R *et al* 2019 *DTT—Divertor Test Tokamak—Interim Design Report* (ENEA)
[2] Ambrosino R 2021 DTT—Divertor Tokamak Test facility: a testbed for DEMO *Fusion Eng. Des.* **167** 112330
[3] Pericoli Ridolfini V, Chmielewski P, Ivanova-Stanik I, Poradziński M, Zagórski R, Ambrosino R and Crisanti F 2020 Comparison between liquid lithium and liquid tin targets in reactor relevant conditions for DEMO and I-DTT *Phys. Plasmas* **27** 112506
[4] Nallo G F, Mazzitelli G, Savoldi L, Subba F and Zanino R 2019 Self-consistent modelling of a liquid metal box-type divertor with application to the divertor tokamak test facility: Li versus Sn *Nucl. Fusion* **59** 066020
[5] Moscheni M *et al* 2022 Cross-code comparison of the edge codes SOLPS-ITER, SOLEDGE2D and UEDGE in modelling a low-power scenario in the DTT *Nucl. Fusion* **62** 056009
[6] Balbinot L, Rubino G and Innocente P 2021 Development of DTT single null divertor scenario *Nucl. Mater. Energy* **27** 100952
[7] Zagórski R, Ivanova-Stanik I, Pericoli Ridolfini V, Poradziński M and Crisanti F 2019 Preliminary integrated core-SOL-divertor modelling for DTT tokamak with liquid metal divertor targets *Fusion Eng. Des.* **146** 1916–20
[8] Zagórski R, Pericoli Ridolfini V, Subba F, Crisanti F, Giruzzi G, Reimerdes H and Rubino G 2017 The DTT device: power and particle exhaust *Fusion Eng. Des.* **122** 313–21
[9] Zagórski R, Ivanova-Stanik R I and Stankiewicz R 2013 *Nucl. Fusion* **53** 073030
[10] Ivanova-Stanik I, Zagórski R, Telesca G, Czarnecka A, Challis C and Hobirk J (JET EFDA Contributors) 2014 Integrated modelling of nitrogen seeded JET ILW discharges for H-mode and hybrid scenarios *Contrib. Plasma Phys.* **54** 4–6
[11] Zagórski R, Ivanova-Stanik I, Czarnecka A, Telesca G and Brezinsek S 2015 Influence of seeding and SOL transport on plasma parameters in JET ITER-like wall H-mode discharges *J. Nucl. Mater.* **463** 649–53
[12] Ivanova-Stanik I, Zagórski R, Chomiczewska A, Bernert M, Glöggler S and Kallenbach A 2022 COREDIV modelling of nitrogen and krypton seeding at the ASDEX Upgrade tokamak *Plasma Phys. Control. Fusion* **64** 045015

[13] Braginskii S I 1965 *Rev. Plasma Phys.* **1** 205
[14] Yamamura Y *et al* 1983 *Report* IPPJ-AM-26(1083) (Institute of Plasma Physics Nagoya)
[15] Casiraghi I *et al* 2021 First principle-based multi-channel integrated modelling in support of the design of the Divertor Tokamak Test facility *Nucl. Fusion* **61** 116068
[16] Casiraghi I *et al* 2021 Integrated modelling of the main Divertor Tokamak Test facility scenarios *47th EPS Conf. on Plasma Physics* (*virtual conf.,21–25 June*) p P2.1078
[17] Ivanova-Stanik I, Zagórski R, Chomiczewska A, Lomas P J, Voitsekhovitch I, Ferreira D R, Sozzi C, Joffrin E and Lerche E 2021 Influences of heating and plasma density on impurity production and transport during the ramp-down phase of JET ILW discharge *Plasma Phys. Control. Fusion* **63** 035008
[18] Ivanova-Stanik I, Challis C D, Chomiczewska A, Hobirk J, Huber A, Kappatou A, Lerche E, Telesca G and Zagórski R (JET Contributors) 2022 Influence of the impurities in the hybrid discharges with high power in JET ILW *Nucl. Fusion* **62** 066010
[19] Kukushkin A S, Pacher H D, Pacher G W, Kotov V, Pitts R A and Reiter D 2013 Consequences of a reduction of the upstream power SOL width in ITER *J. Nucl. Mater.* **438** S203–7
[20] Ivanova-Stanik I, Zagórski R, Voitsekhovitch I and Brezinsek S 2016 Influence of impurity seeding on plasma burning scenarios for ITER *Fusion Eng. Des.* **109–111** 342–6
[21] Chankin A V *et al* 2006 SOLPS modelling of ASDEX upgrade H-mode plasma *Plasma Phys. Control. Fusion* **48** 839–68
[22] Gałazka K, Ivanova-Stanik I, Bernert M, Czarnecka A, Kallenbach A and Zagörski R (ASDEX Upgrade Team) 2016 Impurity seeding in ASDEX Upgrade tokamak modeled by COREDIV code *Contrib. Plasma Phys.* **56** 772–7
[23] Martin Y R, Takizuka T and (The ITPA CDBM H-mode Threshold Database Working Group) 2008 *J. Phys.: Conf. Ser.* **123** 012033
[24] Kallenbach A *et al* 2015 Partial detachment of high power discharges in ASDEX Upgrade *Nucl. Fusion* **55** 053026
[25] Ivanova-Stanik I, Poradziński M, Zagórski R and Siccinio M 2019 Analyses of the influence of the recycling coefficient on He confinement in DEMO reactor *Fusion Eng. Des.* **146** 2021